nature genetics

Mutation of *NLRC4* causes a syndrome of enterocolitis and autoinflammation

Neil Romberg[1,9], Khatoun Al Moussawi[2,9], Carol Nelson-Williams[3,4], Amy L Stiegler[5], Erin Loring[3], Murim Choi[3,4], John Overton[3], Eric Meffre[2,6], Mustafa K Khokha[1,3], Anita J Huttner[7], Brian West[7], Nikolai A Podoltsev[2], Titus J Boggon[5], Barbara I Kazmierczak[2,8,10] & Richard P Lifton[2–4,10]

Upon detection of pathogen-associated molecular patterns, innate immune receptors initiate inflammatory responses. These receptors include cytoplasmic NOD-like receptors (NLRs) whose stimulation recruits and proteolytically activates caspase-1 within the inflammasome, a multiprotein complex. Caspase-1 mediates the production of interleukin-1 family cytokines (IL1FCs), leading to fever and inflammatory cell death (pyroptosis)[1,2]. Mutations that constitutively activate these pathways underlie several autoinflammatory diseases with diverse clinical features[3]. We describe a family with a previously unreported syndrome featuring neonatal-onset enterocolitis, periodic fever, and fatal or near-fatal episodes of autoinflammation. We show that the disease is caused by a *de novo* gain-of-function mutation in *NLRC4* encoding a p.Val341Ala substitution in the HD1 domain of the protein that cosegregates with disease. Mutant NLRC4 causes constitutive IL1FC production and macrophage cell death. Infected macrophages from affected individuals are polarized toward pyroptosis and exhibit abnormal staining for inflammasome components. These findings identify and describe the cause of a life-threatening but treatable autoinflammatory disease that underscores the divergent roles of the NLRC4 inflammasome.

Secretion of IL1FCs (IL-1 and IL-18) normally requires two signals. 'Signal 1', from membrane-spanning receptors (for example, Toll-like receptors), induces the expression of pro-IL1FCs[2]. 'Signal 2', from cytosolic detectors including NLRs, leads to procaspase-1 autoproteolysis and activation[1]. Cleaved caspase-1 converts pro-IL1FCs into their active forms[2,4]. One NLR, NLRC4, cooperates with NAIP to detect flagellin and components of the type 3 secretion system (TTSS), used by *Salmonella typhimurium* and *Pseudomonas aeruginosa* to infect host cells[5,6]. Upon ligand binding, NAIP and NLRC4 oligomerize and recruit the adaptor protein ASC (apoptosis-associated speck-like protein containing a CARD)[7,8]. This macromolecular NLRC4 inflammasome (>1 μm in diameter) induces autoproteolysis of procaspase-1, with subsequent IL1FC secretion and pyroptosis[1,7]. Mutant mice that cannot colocalize ASC and cleaved caspase-1 lose the ability to produce IL1FCs yet retain pyroptosis[6,9,10].

The index case in our study (**Fig. 1a**, III.3) presented at 1 week of life with secretory diarrhea and fever (38.8 °C); no infectious cause was identified. Markers of systemic inflammation were at elevated levels, including ferritin (4,840 ng/ml; normal range of 18–370 ng/ml) (**Fig. 1d**) and C-reactive protein (**Supplementary Table 1**). The numbers of natural killer (NK) cells were reduced. Hypertriglyceridemia, hypofibrinoginemia, coagulopathy and pancytopenia developed, culminating in death on day 23 from diffuse alveolar hemorrhage. Autopsy found splenomegaly, numerous activated (CD163-positive) macrophages infiltrating the central nervous system (**Supplementary Fig. 1**) and widespread bowel autolysis. Remaining intestinal tissue showed the presence of mixed inflammatory cells and villous blunting (**Fig. 1b**, top).

Two days after the funeral for the index case, his 43-year-old father (**Fig. 1a**, II.3) presented with fever (40.6 °C), acute respiratory distress syndrome, subarachnoid hemorrhage and hematochezia; disseminated intravascular coagulation and pancytopenia developed, with elevated levels of ferritin (29,200 ng/ml), IL-18 (11,934 pg/ml; normal range of 69–503 pg/ml), C-reactive protein and soluble IL-2R (**Supplementary Table 1**). Bone marrow biopsy showed erythro- and myelophagocytosis (**Fig. 1c**). Ultrasonography showed splenomegaly. NK cell lymphopenia was prominent. As no infectious agent was isolated, high-dose intravenous immunoglobulin, dexamethasone and cyclosporine were instituted for immunosuppression. The father gradually improved and was discharged after 9 weeks, remaining on cyclosporine; serum ferritin levels normalized, but IL-18 levels remained markedly elevated (**Fig. 1d,e**). He subsequently reported a lifelong history of periodic fevers (>40 °C) provoked

[1]Department of Pediatrics, Yale University School of Medicine, New Haven, Connecticut, USA. [2]Department of Internal Medicine, Yale University School of Medicine, New Haven, Connecticut, USA. [3]Department of Genetics, Yale University School of Medicine, New Haven, Connecticut, USA. [4]Howard Hughes Medical Institute, Yale University School of Medicine, New Haven, Connecticut, USA. [5]Department of Pharmacology, Yale University School of Medicine, New Haven, Connecticut, USA. [6]Department of Immunobiology, Yale University School of Medicine, New Haven, Connecticut, USA. [7]Department of Pathology, Yale University School of Medicine, New Haven, Connecticut, USA. [8]Department of Microbial Pathogenesis, Yale University School of Medicine, New Haven, Connecticut, USA. [9]These authors contributed equally to this work. [10]These authors jointly directed this work. Correspondence should be addressed to R.P.L. (richard.lifton@yale.edu) or B.I.K. (barbara.kazmierczak@yale.edu).

Received 5 May; accepted 23 July; published online 14 September 2014; doi:10.1038/ng.3066

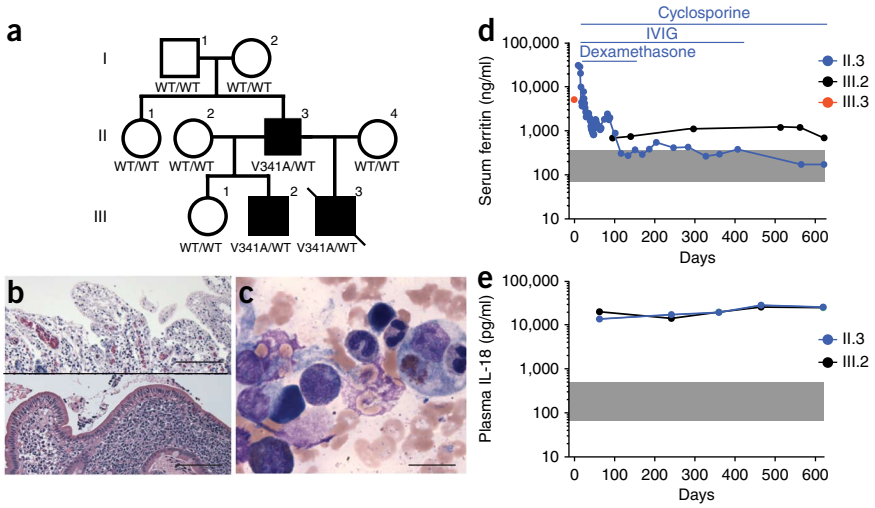

Figure 1 Kindred with a syndrome of infantile enterocolitis and autoinflammation caused by mutation of *NLRC4*. (**a**) Kindred structure. Affected members are denoted by filled symbols. Protein alterations encoded at the *NLRC4* locus are indicated. WT, wild type. (**b**) Hematoxylin and eosin staining of duodenal tissue obtained by autopsy (top; subject III.3) or biopsy (bottom; subject III.2) demonstrating villous blunting and the presence of intraepithelial lymphocytes. Original magnification, 200×; scale bars, 500 µm. (**c**) Hematoxylin and eosin staining of bone marrow from subject II.3 during an episode of acute autoinflammation demonstrating hemo- and myelophagocytosis. Original magnification, 1,000×; scale bar, 20 µm. (**d**) Elevated serum ferritin concentrations in three affected individuals. The immune-modulatory treatments used in subject II.3 (blue) are indicated. The institutional normal range is indicated in gray. $t = 0$ represents the birth date of subject III.3. The father (II.3) presented with acute illness at day 28. Subject III.2 has been interictal during laboratory assessments and without severe febrile episodes throughout the observed interval. IVIG, intravenous administration of immunoglobulin G. (**e**) Elevated plasma IL-18 levels in subjects II.3 and III.2. The normal range, indicated in gray, was determined by testing the plasma of 4 related (3 adult, 1 pediatric) and 18 unrelated (13 adult, 5 pediatric) healthy controls.

by physical and emotional stressors. During infancy, he had an extended hospitalization for fever, vomiting, non-bloody diarrhea and failure to thrive; no specific diagnosis was made. His gastrointestinal symptoms resolved by 1 year of age. In adulthood, erythematous plaques and joint pains accompanied fevers; sero-negative psoriatic arthritis was diagnosed.

The father's family history included healthy parents and two additional offspring, one without illness and a 5-year-old half-brother (III.2) of the deceased infant (III.3) who also had periodic fevers (range of 38.9–40 °C) beginning on day 3 of life after circumcision. A more severe febrile episode associated with vomiting, non-hemolytic anemia and acute renal failure occurred at 6 weeks of age (**Supplementary Table 1**). Later, his fevers were induced by overexertion and were accompanied by abdominal pain. A duodenal biopsy in the first year of life found villous blunting and the presence of intraepithelial lymphocytes (**Fig. 1b**, bottom). The levels of inflammatory markers including ferritin (516–856 ng/ml), C-reactive protein, soluble IL-2R and plasma IL-18 (11,520–24,129 pg/ml) were persistently elevated (**Fig. 1d**,**e**). NK cells, normal in number, were dysfunctional as determined by chromium release assay (**Supplementary Table 1**). Clinical signs of chronic inflammation included short stature (<3rd percentile for height and weight) and recurrent myalgias.

During the index case's acute illness, the possibility of a new genetic syndrome was considered, leading to exome sequencing of the index case and his parents (Online Methods). Clinical features suggesting hemophagocytic lymphohistiocytosis led to the examination of genes implicated in this syndrome[11]; no rare variants were identified (**Supplementary Table 2**). Upon the father's illness, 34 new protein-altering variants (absent in dbSNP, 1000 Genomes Project, National Heart, Lung, and Blood Institute (NHLBI) and Yale exome databases) shared by the index case and his father were identified, including 6 occurring at positions that were invariant among orthologs (**Supplementary Table 3**). Whereas none of the altered genes cause known inflammatory diseases, one variant was identified in *NLRC4*, which encodes a core inflammasome protein. This variant encoding a p.Val341Ala substitution affected helical domain 1 (HD1), which provides a 'lid' to the nucleotide-binding domain (NBD) for ADP in the crystal structure of inactive NLRC4 (**Fig. 2**). Ligand binding normally opens this structure, leading to the exchange of ATP for ADP, thereby promoting oligomerization and inflammasome assembly[12]. Gain-of-function mutations affecting the NBD of the related protein NLRP3 cause constitutive NLRP3 inflammasome assembly, resulting in the production of IL-1β, fever and a spectrum of autoinflammatory disorders—the cryopyrinopathies[13–15]. These diseases are clinically distinct from the disease in our family as the cryopyrinopathies lack gastrointestinal pathology[16].

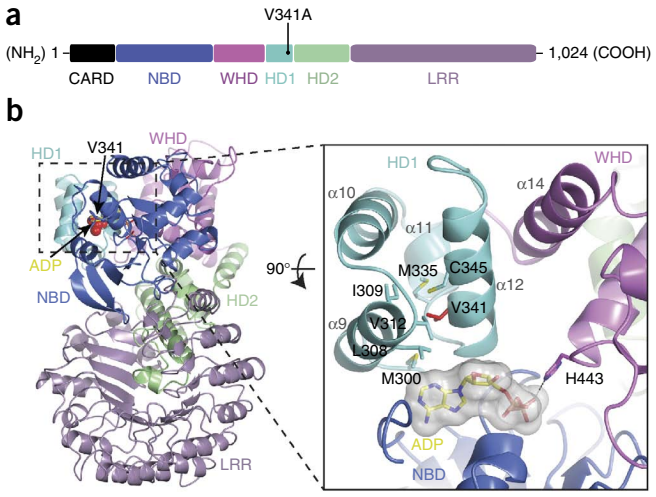

Figure 2 The p.Val341Ala amino acid substitution is positioned within the HD1 domain of NLRC4. (**a**) A schematic of the NLRC4 protein with the individual domains labeled: CARD, caspase activation and recruitment domain; NBD, nucleotide-binding domain; WHD, winged-helix domain; HD1, helicase domain 1; HD2, helicase domain 2; LRR, leucine-rich domain. The location of the p.Val341Ala substitution is displayed. (**b**) Mapping of Val341 onto the crystal structure of mouse NLRC4 in the ADP-bound state (Protein Data Bank (PDB) accession 4KXF)[12,25]. The ribbon diagram excludes the N-terminal CARD domain, which was not included in the crystal structure. ADP is drawn as sticks, and the position of Val341 is indicated with red spheres. The zoomed-in region (with the structure rotated 90° toward the reader) shows the position of Val341 on helix α12. Neighboring hydrophobic residues within the HD1 domain (black outlines) and adjacent α helices are numbered.

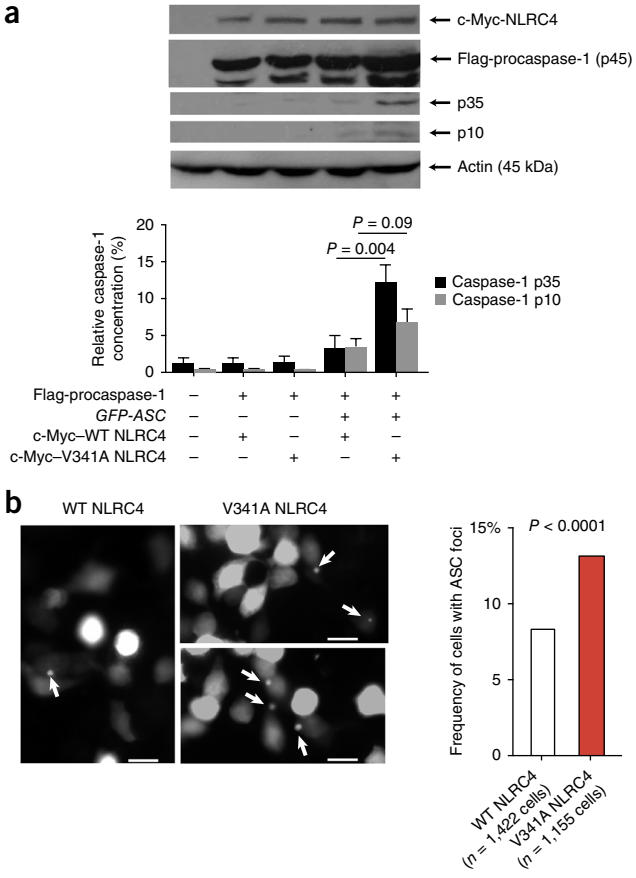

Figure 3 Val341Ala NLRC4 promotes the spontaneous cleavage of procaspase-1 and ASC multimerization in HEK293 cells. (**a**) Increased cleavage of Flag-tagged procaspase-1 in HEK293 cells expressing Val341Ala versus wild-type NLRC4. Top, the protein blot shows the results of blotting for NLRC4, procaspase-1 (p45) and its p35 and p10 cleavage products, as well as actin control, in cells expressing the constructs indicated below (Online Methods). Bottom, the bar graph shows the mean and s.d. of four independent transfections. The levels of p35 and p10 were normalized in each case to the level of procaspase-1. Alternate analysis normalizing p35 and p10 levels to the level of actin or NLRC4 also yielded statistically significant differences between lines transfected with constructs for wild-type and Val341Ala NLRC4. A two-sided Student's *t* test was used to determine statistical significance. (**b**) Spontaneous ASC multimerization (white arrows) in HEK293 cells expressing GFP-ASC and either wild-type NLRC4 or Val341Ala NLRC4 using epifluorescent microscopy. A total of 1,422 cells transfected with construct for wild-type NLRC4 and 1,155 cells transfected with construct for mutant NLRC4 were scored. The significance of differences in the frequency of ASC puncta–positive cells in wild-type and mutant cells was evaluated by χ^2 test. Scale bars, 20 µm.

Evaluation of the *NLRC4* variant encoding p.Val341Ala in the extended family demonstrated that it occurred *de novo* in the affected father and cosegregated with the inflammatory disease (**Fig. 1a**). None of the five other new variants at conserved positions showed cosegregation with disease or *de novo* origin. The finding of a *de novo* mutation in *NLRC4*, which cosegregates with a consistent clinical syndrome and biomarkers of inflammasome activation, provides strong evidence that the *NLRC4* mutation encoding p.Val341Ala causes this syndrome (syndrome of enterocolitis and autoinflammation associated with mutation in *NLRC4*, or SCAN4).

To evaluate the consequence of the NLRC4 p.Val341Ala substitution, we cotransfected constructs encoding wild-type or mutant human NLRC4 into HEK293 cells along with constructs encoding human ASC and caspase-1 and measured the cleavage of procaspase-1. As anticipated, the cleavage of procaspase-1 was dependent on the presence of ASC (**Fig. 3a** and ref. 6). In comparison to cells expressing wild-type NLRC4, cells that expressed Val341Ala NLRC4 showed a fourfold increase in the spontaneous production of the caspase-1 p35 cleavage product (P = 0.004; **Fig. 3a**). Assembled inflammasomes form discrete foci in cells. We counted GFP-tagged ASC foci in cells expressing wild-type or Val341Ala NLRC4. These foci were more frequently present in cells expressing mutant NLRC4 than in those expressing wild-type protein (12.3% versus 7.6%; $P < 0.0001$) (**Fig. 3b**). Multiple ASC foci were not observed in any transfected HEK293 cells.

We investigated constitutive NLRC4 inflammasome activation in macrophages derived from the peripheral blood monocytes of SCAN4 cases (II.3 and III.2) and healthy related ($n = 1$) and unrelated ($n = 4$) controls. Without signal 2 (that is, NLR ligand), control macrophages did not form ASC foci nor did they stain with biotin-YVAD-FMK (which binds activated caspase-1; **Supplementary Fig. 2a,b**). In contrast, 3.3% of SCAN4 macrophages spontaneously formed ASC foci and 25.9% showed biotin-YVAD-FMK staining, similar to HEK293 cells transfected with construct for Val341Ala NLRC4 (**Fig. 3b** and **Supplementary Fig. 2a,b**).

We cultured case-derived or healthy donor–derived macrophages for 18 h with signal 1 provocation (1 ng/ml lipopolysaccharide (LPS)). As expected, without signal 2, healthy control macrophages showed no detectable secretion of IL-1β (<1.4 pg/ml) and small amounts of IL-18 (22 pg/ml). In contrast, macrophages from both SCAN4 cases (II.3 and III.2) secreted markedly higher IL-1β (76 pg/ml) and IL-18 (212 pg/ml) levels ($P < 0.0001$ in comparison to controls for both; **Fig. 4a,b**).

We measured cell death–associated lactate dehydrogenase (LDH) release in the same 18-h culture supernatants. Macrophages from SCAN4 cases released more LDH than those from healthy controls (12.3% versus 4.7% of the total LDH released during cell death; $P < 0.0001$) (**Fig. 4c**). Addition of Z-YVAD-FMK, which inhibits the catalytic site of cleaved caspase-1, significantly reduced the secretion of IL1FCs but did not reduce cell death (**Supplementary Fig. 3a,b**).

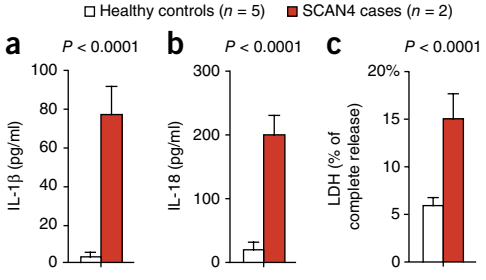

Figure 4 Increased production of IL-1β and IL-18, and increased cell death in macrophages harboring NLRC4 p.Val341Ala. (**a**–**c**) Monocyte-derived macrophages from SCAN4 cases (II.3 and III.2) and wild-type controls (one related and four unrelated) were cultured for 18 h in medium containing low-dose LPS (1 ng/ml), and IL-1β (**a**), IL-18 (**b**) and LDH (**c**) levels were measured (Online Methods). LDH release is reported relative to the result following total cell lysis by Triton X-100 (0.1%). Cytokine secretion and cell death results were similar in macrophages from the cases (II.3 and III.2). Bar graphs show the mean ± s.e.m. from three separate experiments. Significance by unpaired Student's *t* test is indicated.

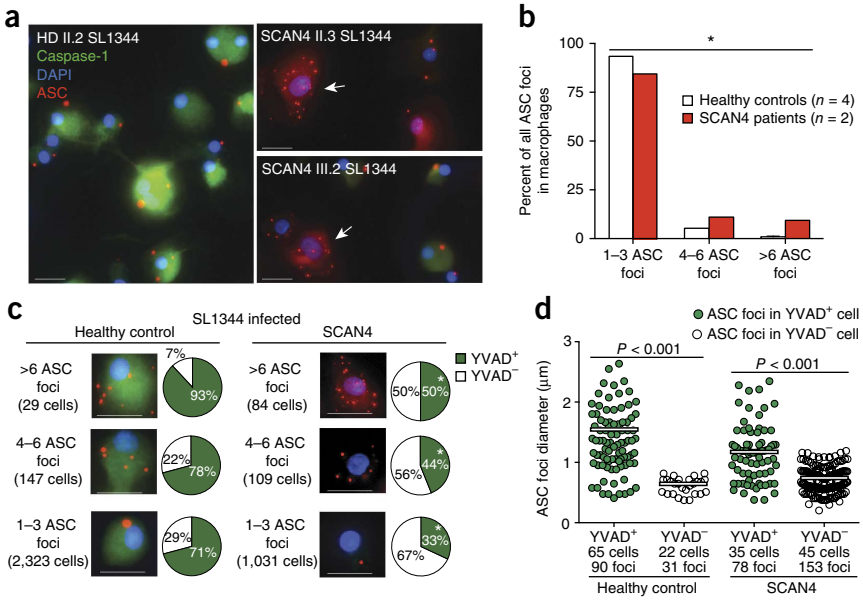

Figure 5 Macrophages from SCAN4 cases infected with *S. typhimurium* strain SL1344 show abnormal ASC staining and limited activation of caspase-1. (**a**) The majority of *S. typhimurium*–infected monocyte-derived macrophages from a representative healthy control (HD II.2, the mother of SCAN4 case III.2) display features of conventional macrophage activation, including biotin-YVAD-CMK staining (green cytoplasmic staining) and a limited number (1–3) of ASC foci (red puncta) per cell. A subset of *S. typhimurium*–infected macrophages (white arrows) from SCAN4 cases II.3 and III.2 display numerous (>6) ASC foci but more limited staining for biotin-YVAD-CMK. DAPI, 4′,6-diamidino-2-phenylindole. Scale bars, 20 µm. (**b**) Quantification of ASC foci in 2,499 *S. typhimurium*–infected macrophages from healthy controls and 1,224 *S. typhimurium*–infected macrophages from cases. (**c**) Representative biotin-YVAD-CMK staining in *S. typhimurium*–infected macrophages from healthy controls or SCAN4 cases from groups with either 1–3, 4–6 or >6 ASC foci/cell. Pie charts display the frequency of cells positive for biotin-YVAD-CMK staining per group. The total number of cells analyzed in each group is given in parentheses. Macrophages in **c** were stained as described in **a**. Scale bars, 20 µm. (**d**) Diameter of ASC foci in macrophages positive (filled green circles) and negative (unfilled circles) for biotin-YVAD-CMK staining from healthy controls and SCAN4 cases II.3 and III.2. Mean foci diameter is displayed as white bars. In **b** and **c**, asterisks denote $P < 0.0001$ in cases versus controls by χ^2 test. Significance by unpaired Student's *t* test is indicated for **d**.

Thus, the NLRC4 p.Val341Ala substitution results in gain of function, eliminating the requirement for signal 2 in the activation of caspase-1 and production of IL1FCs. The NLRC4 p.Val341Ala alteration also promotes pyroptosis independently of caspase-1 cytokine processing.

We next infected LPS-primed healthy control– or case-derived macrophages with either of two flagellated, TTSS-positive pathogens, *S. typhimurium* (strain SL1344) or *P. aeruginosa* (strain PAKΔSTY), thus providing both with signal 1 and signal 2 provocation. As anticipated, LPS-primed macrophages from healthy controls secreted abundant IL1FCs and initiated pyroptosis upon infection (**Supplementary Fig. 4a**,**b**). Responses were reduced when cells were infected with *P. aeruginosa* strain PAKΔ*popD*, which lacks a functional TTSS (**Supplementary Fig. 4a**,**b**). In contrast, macrophages derived from SCAN4 cases secreted significantly less IL1FCs upon infection with the pathogenic strains yet showed more cell death than the macrophages from healthy controls (**Supplementary Fig. 4a**,**b**).

Infected macrophages form inflammasomes microscopically identifiable as ASC foci that colocalize with caspase-1. Consistent with published reports using mouse macrophages[9,17], we found that 93% of *S. typhimurium*–infected and 97% of *P. aeruginosa* PAKΔSTY–infected macrophages from healthy controls formed 1–3 large-diameter (>1-µm) ASC foci (**Fig. 5a**, left, **Fig. 5b**, **Supplementary Fig. 5a**, left, and **Supplementary Fig. 5b**). Most cells infected with *S. typhimurium* (71%) or *P. aeruginosa* PAKΔSTY (67%) with 1–3 ASC foci showed caspase-1 proteolysis, indicated by diffuse cytoplasmic biotin-YVAD-CMK staining (**Fig. 5a**, left, **Fig. 5c**, **Supplementary Fig. 5a**, left, and **Supplementary Fig. 5c**). Consistent with previous reports[17,18], ASC foci in most *S. typhimurium*–infected cells from healthy donors colocalized with aggregates of activated caspase-1 (**Supplementary Fig. 6**). A small percentage of cells from healthy donors (1.1% of *S. typhimurium*–infected control macrophages) had >6 ASC foci per cell; 93% of these stained with biotin-YVAD-FMK (**Fig. 5a**, left, and **Fig. 5c**). None of the *P. aeruginosa* PAKΔSTY–infected cells had >6 ASC foci (**Supplementary Fig. 5a**, left, and **Fig. 5c**). In contrast, macrophages derived from SCAN4 cases more frequently had >6 ASC foci (6.8% for *S. typhimurium*–infected and 5.6% for *P. aeruginosa* PAKΔSTY–infected macrophages; each $P < 0.0001$ in comparison to controls). Rare macrophages had more than 20 ASC foci (**Fig. 5a**, right, **Fig. 5b**, **Supplementary Fig. 5a**, right, and **Supplementary Fig. 5b**). Caspase-1 activation was generally limited in infected macrophages derived from SCAN4 cases. Even in macrophages displaying >6 foci, only 50% infected with *S. typhimurium* and 44% infected with *P. aeruginosa* PAKΔSTY displayed diffuse cytoplasmic biotin-YVAD-CMK staining ($P < 0.0001$ and $P = 0.0012$ in comparison to control cells, respectively) (**Fig. 5a**, right, **Fig. 5c**, **Supplementary Fig. 5**, right, and **Supplementary Fig. 5c**). In contrast to the ASC foci in control cells, those in *S. typhimurium*–infected cells from SCAN4 cases did not colocalize with aggregates of activated caspase-1 (**Supplementary Fig. 6**). Lastly, ASC foci in macrophages negative for biotin-YVAD-CMK staining were significantly smaller than those in cells positive for biotin-YVAD-CMK staining for both healthy controls and SCAN4 cases (**Fig. 5d** and **Supplementary Fig. 5d**).

These findings describe a previously unreported mendelian autoinflammatory syndrome featuring periodic fever, neonatal-onset enterocolitis and high levels of IL1FCs and demonstrate its causation by a gain-of-function mutation in *NLRC4*. Like NLRP3 cryopyrinopathies[14], SCAN4 is associated with the constitutive activation of caspase-1 and production of IL1FCs. In the inhibited, ADP-bound state, Val341 of NLRC4 makes van der Waals contacts with the side chains of an adjacent helix in the HD1 domain, comprising the lid on the nucleotide-binding site. The decreased hydrophobicity of the alteration to Ala341 might reduce this interaction, allowing more movement of helix α12 and promoting the exchange of ATP for ADP, either by favoring the open conformation of NLRC4 or by disrupting the stabilizing interaction of His443 with the β phosphate of ADP (**Fig. 2**). Either possibility would promote ligand-independent activation of NLRC4. It is compelling that Canna *et al.*[19] have identified an independent *de novo* mutation in *NLRC4*, encoding a p.Thr337Ser

substitution. The identification of two *de novo* mutations in close proximity in the same gene that segregate with a new clinical phenotype provides strong support for a causal relationship of the mutations with pathogenesis.

SCAN4 is distinctive from NLRP3 cryopyrinopathies in its association with neonatal-onset enterocolitis. This clinical feature might relate to *NLRC4* being highly expressed in intestinal macrophages whereas *NLRP3* is not[20]. It is interesting that the marked enterocolitis of each surviving SCAN4 case resolved by 1 year of age. We speculate that the chronic inflammatory state might be exacerbated in the infant gut by constant signal 1 provocation from newly acquired symbionts. As host-microbe interactions mature, the presence of microflora with decreased capacity to induce inflammation might account for reduced gut inflammation[21].

IL-1β–targeted drugs are approved for the treatment of NLRP3 cryopyrinopathies[22–24]. We expect that IL-1β blockade will be similarly effective in individuals with SCAN4. Although both surviving members in our family have presently declined interictal therapy, the complementary report by Canna *et al.* provides evidence for the efficacy of IL-1 receptor blockade[19].

Macrophages derived from SCAN4 cases show high levels of IL1FC secretion and increased cell death with signal 1, despite the absence of signal 2; addition of signal 2 frequently results in the formation of multiple ASC foci with increased cell death, despite blunted IL1FC secretion. One possible explanation for these observations is that mutant NLRC4 promotes traditional inflammasome assembly in the absence of signal 2 provocation but intracellular ligand binding promotes the formation of ASC foci that lack activated caspase-1, resulting in smaller structures with an impaired ability to produce cytokines. This proposal is supported by findings from experiments in mice with mutated inflammasome components [6,9,10], which demonstrated defective cytokine processing yet intact pyroptosis. Modulating the balance between cytokine production and pyroptosis might determine the distinct states of subclinical autoinflammation, periodic fever, and fatal or near-fatal autoinflammation seen in individuals with SCAN4.

METHODS

Methods and any associated references are available in the online version of the paper.

Accession codes. The *NLRC4* mutation encoding p.Vall341Ala has been deposited in the NCBI ClinVar database under accession SCV000172282.

Note: Any Supplementary Information and Source Data files are available in the online version of the paper.

ACKNOWLEDGMENTS

We thank the patients and their families for their participation. We thank the Yale pediatric and medicine intensive care teams for providing access to patients. We thank the staff of the Yale Center for Genome Analysis for the generation of the exome sequence data and the Yale Center for Clinical Investigation for statistical assistance. We thank C. Roy (Yale School of Medicine) for the *CASP1* and *ASC* constructs and L. Devine for multiplex cytokine detection. This work was supported by grants K12HD0141401-10 (US National Institutes of Health/National Institute of Child Health and Human Development) to N.R., U54HG006504 01 (Yale Center for Mendelian Genomics) to R.P.L. and R01AI081825 (US National Institutes of Health/National Institute of Allergy and Infectious Diseases) to B.I.K. B.I.K. is a Burroughs Wellcome Fund Investigator in the Pathogenesis of Infectious Diseases.

AUTHOR CONTRIBUTIONS

R.P.L., B.I.K., N.R. and K.A.M. designed the study and experiments. K.A.M. and N.R. performed cellular and molecular experiments. N.R., N.A.P., M.K.K. and E.L. identified, consented and recruited study subjects and provided clinical information. B.W. and A.J.H. provided autopsy and/or biopsy interpretations and images. C.N.-W., J.O. and M.C. generated and analyzed sequencing data. T.J.B. and A.L.S. generated and interpreted three-dimensional alteration maps for NLRC4. N.R. and E.M. processed case samples. N.R., R.P.L. and B.I.K. wrote the manuscript.

COMPETING FINANCIAL INTERESTS

The authors declare no competing financial interests.

1. Mariathasan, S. & Monack, D.M. Inflammasome adaptors and sensors: intracellular regulators of infection and inflammation. *Nat. Rev. Immunol.* **7**, 31–40 (2007).
2. Dinarello, C.A. Immunological and inflammatory functions of the interleukin-1 family. *Annu. Rev. Immunol.* **27**, 519–550 (2009).
3. Ozen, S. & Bilginer, Y. A clinical guide to autoinflammatory diseases: familial Mediterranean fever and next-of-kin. *Nat. Rev. Rheumatol.* **10**, 135–147 (2014).
4. Thornberry, N.A. *et al.* A novel heterodimeric cysteine protease is required for interleukin-1β processing in monocytes. *Nature* **356**, 768–774 (1992).
5. Miao, E.A. *et al.* Cytoplasmic flagellin activates caspase-1 and secretion of interleukin 1β via Ipaf. *Nat. Immunol.* **7**, 569–575 (2006).
6. Sutterwala, F.S. *et al.* Immune recognition of *Pseudomonas aeruginosa* mediated by the IPAF/NLRC4 inflammasome. *J. Exp. Med.* **204**, 3235–3245 (2007).
7. Martinon, F., Burns, K. & Tschopp, J. The inflammasome: a molecular platform triggering activation of inflammatory caspases and processing of proIL-β. *Mol. Cell* **10**, 417–426 (2002).
8. Mariathasan, S. *et al.* Differential activation of the inflammasome by caspase-1 adaptors ASC and Ipaf. *Nature* **430**, 213–218 (2004).
9. Broz, P., von Moltke, J., Jones, J.W., Vance, R.E. & Monack, D.M. Differential requirement for caspase-1 autoproteolysis in pathogen-induced cell death and cytokine processing. *Cell Host Microbe* **8**, 471–483 (2010).
10. Miao, E.A. *et al.* Caspase-1–induced pyroptosis is an innate immune effector mechanism against intracellular bacteria. *Nat. Immunol.* **11**, 1136–1142 (2010).
11. Jordan, M.B., Allen, C.E., Weitzman, S., Filipovich, A.H. & McClain, K.L. How I treat hemophagocytic lymphohistiocytosis. *Blood* **118**, 4041–4052 (2011).
12. Hu, Z. *et al.* Crystal structure of NLRC4 reveals its autoinhibition mechanism. *Science* **341**, 172–175 (2013).
13. Hoffman, H.M., Mueller, J.L., Broide, D.H., Wanderer, A.A. & Kolodner, R.D. Mutation of a new gene encoding a putative pyrin-like protein causes familial cold autoinflammatory syndrome and Muckle-Wells syndrome. *Nat. Genet.* **29**, 301–305 (2001).
14. Agostini, L. *et al.* NALP3 forms an IL-1β–processing inflammasome with increased activity in Muckle-Wells autoinflammatory disorder. *Immunity* **20**, 319–325 (2004).
15. Aksentijevich, I. *et al. De novo CIAS1* mutations, cytokine activation, and evidence for genetic heterogeneity in patients with neonatal-onset multisystem inflammatory disease (NOMID): a new member of the expanding family of pyrin-associated autoinflammatory diseases. *Arthritis Rheum.* **46**, 3340–3348 (2002).
16. Neven, B., Prieur, A.M. & Quartier dit Maire, P. Cryopyrinopathies: update on pathogenesis and treatment. *Nat. Clin. Pract. Rheumatol.* **4**, 481–489 (2008).
17. Fernandes-Alnemri, T. *et al.* The pyroptosome: a supramolecular assembly of ASC dimers mediating inflammatory cell death via caspase-1 activation. *Cell Death Differ.* **14**, 1590–1604 (2007).
18. Man, S.M. *et al.* Inflammasome activation causes dual recruitment of NLRC4 and NLRP3 to the same macromolecular complex. *Proc. Natl. Acad. Sci. USA* **111**, 7403–7408 (2014).
19. Canna, S.W. *et al.* An activating *NLRC4* inflammasome mutation causes autoinflammation with recurrent macrophage activation syndrome. *Nat. Genet.* doi:10.1038/ng.3089 (14 September 2014).
20. Franchi, L. *et al.* NLRC4-driven production of IL-1β discriminates between pathogenic and commensal bacteria and promotes host intestinal defense. *Nat. Immunol.* **13**, 449–456 (2012).
21. Yatsunenko, T. *et al.* Human gut microbiome viewed across age and geography. *Nature* **486**, 222–227 (2012).
22. Lachmann, H.J. *et al.* Use of canakinumab in the cryopyrin-associated periodic syndrome. *N. Engl. J. Med.* **360**, 2416–2425 (2009).
23. Hawkins, P.N., Lachmann, H.J., Aganna, E. & McDermott, M.F. Spectrum of clinical features in Muckle-Wells syndrome and response to anakinra. *Arthritis Rheum.* **50**, 607–612 (2004).
24. Hoffman, H.M. *et al.* Efficacy and safety of rilonacept (interleukin-1 Trap) in patients with cryopyrin-associated periodic syndromes: results from two sequential placebo-controlled studies. *Arthritis Rheum.* **58**, 2443–2452 (2008).
25. Bernstein, F.C. *et al.* The Protein Data Bank. A computer-based archival file for macromolecular structures. *Eur. J. Biochem.* **80**, 319–324 (1977).

ONLINE METHODS

Research subjects. The study protocol was approved by the Yale Human Research Protection Program. Informed consent was provided by all participants or their legal guardians. Clinical data were abstracted from medical records. Tissues from biopsy and autopsy specimens were labeled using standard hematoxylin and eosin staining protocols or by immunohistochemical staining with an antibody to CD163 (ab87099, Abcam; diluted to 5 μg/ml).

Genetic analysis. DNA was prepared from venous blood samples of the index case and kindred members. Exome sequencing of the index case and his parents was performed by capture on the NimbleGen 2.1 Exome reagent followed by 74-bp end sequencing on the Illumina platform to high coverage (each targeted base was read by a mean of more than 80 independent reads in each subject) as previously described[26]. Sequences were aligned to NCBI Build 36 of the human genome, and single-nucleotide variant (SNV) and indel calls were assigned quality scores using SAMtools and annotated for novelty (using Yale, 1000 Genomes Project and NHLBI exome databases), for impact on the encoded proteins and for conservation of variant position as previously described[26]. Variants were sought in genes implicated in hemophagocytic lymphohistiocytosis; none were identified (**Supplementary Table 2**). Thirty-four protein-altering variants that were absent in dbSNP, 1000 Genomes Project, NHLBI and Yale exome databases that were shared by the index case and affected father were identified (**Supplementary Table 3**) and evaluated. Only one was in a gene known to have a role in the activation of the innate immune system (*NLRC4*). Variants in *NLRC4* and in the five other genes in which the new variants occurred at completely conserved positions (*ALK*, *DCC*, *FBXO4*, *KIF13B* and *SLC7A6OS*) were confirmed by PCR amplification followed by Sanger sequencing, and transmission through the complete pedigree was evaluated. The *NLRC4* variant proved to be *de novo* in the affected father and perfectly cosegregated with the autoinflammatory syndrome in the pedigree, whereas the other variants were all transmitted from an unaffected grandparent of the index case and did not cosegregate with disease. The *NLRC4* mutation encoding p.Val341Ala has been deposited in the NCBI ClinVar database (accession SCV000172282).

Functional analysis of p.Val341Ala-altered NLRC4. NLRC4 activity was analyzed in HEK293 cells (from the American Type Culture Collection). Wild-type human *NLRC4* was cloned into pMycB (Santa Cruz Biotechnology) and verified by Sanger sequencing. The c.1022T->C mutation was introduced by site-directed mutagenesis (Stratagene QuikChange) and verified by Sanger sequencing. Constructs for mutant and wild-type Myc-NLRC4 were transiently transfected into HEK293 cells along with constructs encoding human procaspase-1 with an N-terminal Flag tag and GFP-tagged human ASC using Lipofectamine 2000 (Invitrogen). NLRC4 activity was measured visually 30 h after transfection by the spontaneous formation of GFP-ASC foci (as visualized in live cells by epifluorescent microscopy). Manual enumeration of ASC-positive foci was performed over 20 representative fields at 20× magnification. Procaspase-1 p45 autoproteolysis was measured directly by protein blotting for the p35 (anti-Flag M2 (F1804), Sigma; 1:1,000 dilution) and p10 (antibody to caspase-1 p10 (sc-514), Santa Cruz Biotechnology; 1:200 dilution) fragments, using HRP-conjugated secondary antibody to mouse IgG or rabbit IgG (Bio-Rad) and enhanced chemiluminescence. The presence of NLRC4 and actin in lysates was confirmed by blotting with antibody to c-Myc (9E10, Enzo Life Sciences; 1:1,000 dilution) and rabbit pan-actin polyclonal antibody (4970, Cell Signaling Technology; 1:5,000 dilution), respectively. Untransfected cells were used as internal controls.

Functional studies of monocyte-derived macrophages. CD14-positive monocytes were purified from the peripheral blood mononuclear cells of SCAN4 cases and healthy donor controls using magnetic beads with antibody to human CD14 (Miltenyi). Cells from the two living SCAN4 cases were used for all functional studies, whereas the number and relatedness of the healthy donors used varied from experiment to experiment and were based on same-day availability. Monocytes were differentiated into macrophages in RPMI containing 10% FBS and M-CSF (10 ng/ml) over 7 d (ref. 27). Macrophages (2×10^5) were cultured for 18 h in culture medium containing LPS (1 ng/ml) with or without Z-YVAD-FMK (Enzo Life Sciences) at a concentration of 0.1–0.5 μM. Culture supernatants were collected, and cells were washed and recultured with LPS-free medium before infection with *P. aeruginosa* or S. *typhimurium*. PAKΔSTY and SL1344 are flagellated strains that are positive for the TTSS. PAKΔ*popD* is a flagellated strain that does not express a functional TTSS. The construction and characterization of bacterial strains has been described previously[6,28]. Culture supernatants from infected macrophages were collected after 1 h. Secreted IL-1β and IL-18 were measured by ELISA (Millipore and MBL, respectively) for both the 18-h and 1-h culture supernatants. Cell-free LDH levels were measured by ELISA according to the manufacturer's protocol (Takara). The amount of LDH released into supernatants was normalized to the amount of LDH released from macrophages lysed with Triton X-100 (0.1%).

Immunofluorescence microscopy of infected macrophages. Macrophages (2×10^5), differentiated as described above, were plated on glass coverslips. Cells were incubated with 2 μM biotin-YVAD-CMK for 30 min before infection with *P. aeruginosa* PAKΔSTY or PAKΔ*popD* or with S. *typhimurium* SL1344 at a multiplicity of infection of 20 bacteria/cell for 1 h. Cells were fixed with paraformaldehyde (4%), blocked with 1% fish scale gelatin (Sigma) in PBS with 0.1% TX-100, and stained (1:1,000 dilution) with rabbit antibody to ASC (AL177, AdipoGen) and 4′,6-diamidino-2-phenylindole (DAPI, Sigma). A streptavidin–Alexa Fluor 488 conjugate (Invitrogen) and an Alexa Fluor 594–conjugated antibody to rabbit (Life Technologies) were used (1:1,000 dilution for each) for secondary staining. Macrophages were visually inspected for immunofluorescence using an Axiovert 200M microscope. Manual enumeration of ASC-positive and YVAD-positive macrophages was performed over 20 representative fields at 20× magnification. DAPI staining of bacterial DNA was used to confirm macrophage infection. High-detail magnification for phased images at 60× and 100× was performed on a Nikon Eclipse TE2000-S microscope.

26. Zaidi, S. *et al. De novo* mutations in histone-modifying genes in congenital heart disease. *Nature* **498**, 220–223 (2013).
27. Vijayan, D. Isolation and differentiation of monocytes-macrophages from human blood. *Methods Mol. Biol.* **844**, 183–187 (2012).
28. Wangdi, T., Mijares, L.A. & Kazmierczak, B.I. *In vivo* discrimination of type 3 secretion system–positive and –negative *Pseudomonas aeruginosa* via a caspase-1–dependent pathway. *Infect. Immun.* **78**, 4744–4753 (2010).

doi:10.1038/ng.3066